Effectiveness of Laboratory Physical Modeling in Acquiring the Response of Time Domain Induced Polarization (TDIP)

Yatini [1,a,*], Djoko Santoso [2,b], Agus Laesanpura [2,c], and Budi Sulistijo [3,d]

[1]Geophysics Engineering, Universitas Pembangunan Nasional Veteran Yogyakarta
Jalan SWK 104 (North RingRoad), Condongcatur, Yogyakarta 55283, Indonesia
[2] Geophysics Engineering, Institut Teknologi Bandung,
Jalan Ganesha No 10, Bandung 40132, Indonesia
[3]Mining Engineering, Institut Teknologi Bandung,
Jalan Ganesha No 10, Bandung 40132, Indonesia

e-mail: [a]jeng_tini@upnyk.ac.id, [b] dsantoso78@yahoo.com, [c] laesanpura1@yahoo.com,
and [d] budis@mining.itb.ac.id

* Corresponding Author

Abstract

Induced Polarization (IP) is one of the Geophysical methods that utilize the polarization properties of the rocks for metallic mineral exploration. The problems are how to distinguish the metallic minerals deposit based on the chargeability. The physical modeling of IP is used to study the behavior of TDIP response. The study of a simple mathematical model is carried out to obtain the theoretical curves which are presented as the subsurface parameter. These curves are used as a reference to assess the result of physical modeling. The laboratory physical modeling uses a tank model with a size of $(200 \times 100 \times 70)$ cm³, with a block as a target and water as a host medium. The results show laboratory physical modeling which has been made is quietly good. The approximate position and geometry of the target can be identified. The resistivity inversion modeling is sensitive to recognizing the geometry and position, while the chargeability inversion is on the distribution of metallic minerals. The quantitative correlation between chargeability and iron-ore content is obtained by Dipole-dipole and Wenner configuration. Both are connected exponentially, with a different exponential constant for different block targets.

Keywords: *TDIP response, resistivity; chargeability; physical modeling; metal mineral content.*

INTRODUCTION

Metallic minerals are well known as the metal base material and are almost used in industry to meet human needs. Attempts to obtain metallic mineral reserves continue to do. The research of electrical polarization effects in a rock that was developed by Schlumberger in 1911 became the foundation development of Induced Polarization (IP) methods [1,2]. With the development of tools and the theoretical understanding of electrical properties, the method is more reliable than metallic mineral prospecting tools [3–6]. Currently, in metal mineral exploration activities, the use of IP methods becomes a necessity. This method is better than other geophysical methods due to its accuracy in depicting the distribution of polarized regions caused by the

presence of metallic mineral deposits [7,8]. Apart from prospecting for metal minerals, the IP method is also commonly used for geotechnical studies to determine the clay content in the subsurface or the physical properties of the subsurface layer [8-12]. In the IP method, it is known the induced polarization in the time domain hereinafter called Time Domain Induced Polarization (TDIP). The chargeability as TDIP response which is formulated and distinguishes subsurface polarizability is indicative of metallic minerals [5,13].

Physical modeling is widely used by other researchers to obtain a resolution of resistivity in a variety of configurations, examine the disseminated or massive mineral [7], or evaluate the depth penetration in sounding measurement [7,14,15]. Physical modeling can also be used as a reliability examiner of measurement instruments and measurement methods. The use of physical modeling laboratory to determine the behavior of TDIP responses as metal mineral content in the target was done in the study. Preliminary studies showed that the TDIP response resulting from the measurement of physical models is comparable to the level of iron-ore in the target [5,16]. The use of water as the host medium and block target represents the subsurface properties of the medium. The use of Dipole-dipole and Wenner electrode configurations gives an overview of measurement techniques that influence the TDIP response [17]. Results show that the TDIP response surface is caused by these conditions studied, so the TDIP response behavior on physical modeling can be well understood. In this study, mathematical modeling is also used as a reference for assessing the effectiveness of physical modeling in obtaining TDIP response. In addition, inversion modeling is applied to analyze the results of the physical modeling.

The purpose of the physical modeling of the laboratory is to obtain a quantitative relationship between TDIP response and metallic mineral deposits, by analyzing the behavior of TDIP response to changing iron-ore content in the subsurface target. The mathematical formulation is made to the physical model conditions. The goal is to obtain the theoretical curves that present subsurface parameter relationships with TDIP response. Furthermore, these curves are used as a reference and evaluation of the success of the physical modeling laboratory. The success of physical modeling was also evaluated by the results of the inversion Res2Dinv suitability of the condition of the model.

METHOD
Laboratory Physical Modeling Techniques

Laboratory physical model is made in a glass container (tank model) with a size of 200cm x 100cm x 70cm. Stainless steel wire with 1 mm of diameter and 10 cm of length is used as current electrodes. Nonpolarizable electrodes are made from a pen that is contained in a $CuSO_4$ solution. Copper wire is inserted into it as the potential porous pot electrode of Cu-CuSO$_4$. Based on the test result, the porous pot electrode works very well in physical modeling [17]. The current and potential electrodes are set on a wood that has been marked with the same distance, so the point spaces will always fix to make the data acquisition easier. Each electrode is given a number that shows the position of the measurement point. Water is used as a host medium due to its very small chargeability value, which is close to zero [13, 18-20].

The Measurement of TDIP Response

The midpoint of 0 is used as a reference measurement. The target is placed at the midpoint and is positioned 2 cm below the surface of the water. TDIP response measurements use IP-Meter Syscal Junior IRIS Instruments 568 series that can be used to measure chargeability and resistivity. TDIP response measurements were carried out on the surface of the water.
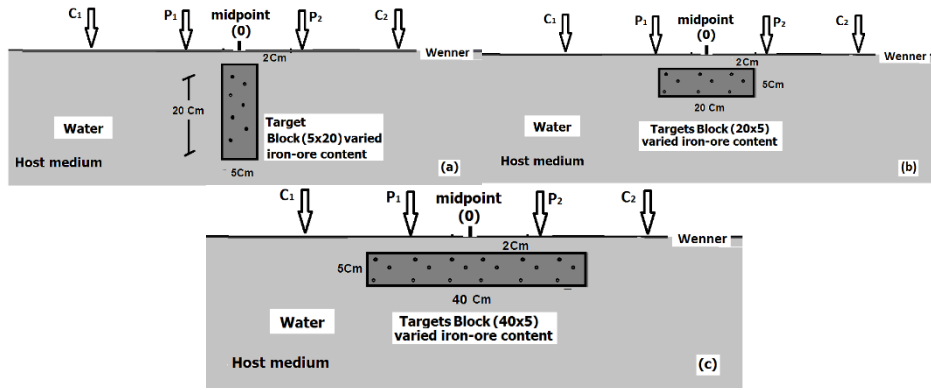
Figure 1. Illustration measurements on physical modeling laboratory with the block target (a) (5x20), (b) (20x5), and (c) (40x5), varying in iron-ore content. Water is used as a host medium. At each target applied Dipole-dipole and Wenner configuration spaced 5cm to get TDIP response data

The whole target applied Dipole-dipole and Wenner configuration spaced 5 cm. Block size (40cmx20cm x5cm) with iron-ore levels of 20%, 40%, 60, 70%, and 80% respectively is used as a target. The measurements illustration can be seen in Figure 1. The data obtained is apparent chargeability and resistivity that were measured at the surface. Meanwhile, the parameter data subsurface shows the true resistivity and chargeability of the host and the target, the target geometry, and measurement electrode arrangement, spacing, and n. Calibration of measuring instruments is carried out as a standard procedure [18]. The true resistivity and chargeability host medium obtained from the measurement of water use Soil Resistivity Box (SRB) as shown in Table 1.

Table 1. The TDIP response value of the target and host medium in the physical modeling laboratory is used as an input in the forward modeling.

Iron-ore content (%)	Fe-total content (%)	Targets		Host medium	
		ϱ (Ohm-m)	m (ms)	ϱ (Ohm-m)	m (ms)
20	7.07	16.18	1.48	36.63	0
40	14.13	16.40	1.97	36.63	0
60	21.20	10.40	1.65	36.63	0
70	24.80	11.20	2.62	36.63	0
80	28.30	8.61	4.23	36.63	0

ϱ = resistivity   m = chargeability

Mathematical Formulation of the Target
The formulation of TDIP response is through the model sphere or block with a host homogeneous isotropic medium. Response due to the target in a homogeneous isotropic medium was obtained by solving the Laplace equation $\nabla^2 V = 0$ with the boundary condition. Settlement for the sphere model with radius R is the IP response of two potentials at the surface.

$$\frac{\rho_a}{\rho_1} = \left[1 + \left(\frac{\rho_1-\rho_2}{\rho_1+2\rho_2}\right)R^3\left(\frac{(2x^2-d^2)}{(x^2+d^2)^{5/2}}\right)\right] \tag{1}$$

$$\frac{m_a}{m_2} = -3\left[\frac{\rho_1^2}{(\rho_1+2\rho_2)^2}\right]R^3\left[\frac{(2x^2-d^2)}{(x^2+d^2)^{5/2}}\right] \tag{2}$$

Where x is the distance of the center of the sphere against the receiving surface, d is the depth of the sphere, ϱ_1, ϱ_2 and m_1, m_2 are resistivity and chargeability on medium and spheres respectively. In addition, m_a, ρ_a are apparent chargeability and resistivity measured surface respectively.

The TDIP responses i.e., resistivity and chargeability (equations 1 and 2) are expressed as a curve which is a description of changes in TDIP response laterally. In this study, the software Res2DMod [21-23] has been selected as the forward modeling process. The forward modeling yield curve describes the relationship between TDIP response to the subsurface parameters and measurement techniques. The theoretical response curves are to be modeled subsurface with the subsurface parameter values and a particular electrode configuration. The data in Table 1 were used as forward modeling. The theoretical TDIP response was obtained for all values of n.

In this study, theoretical curve stimulation results from various spacing at the same depth, while also at different depths in the same spacing. The comparison of these curves can be used to select the appropriate spacing on the desired target depth. The selection of spacing used and the target depth in the laboratory physical modeling is based on the result of stimulation in theoretical curves. The physical modeling laboratory was created from a block target at a depth of 2 cm. TDIP response curves theoretically generate maximum value at 5 cm spacing. Therefore, it is most appropriate when 5 cm in spacing is used [17,24]. The result of theoretical curve stimulation shows that it can be applied in the true field, by paying attention to the selection of the most suitable spacing to find the target with the desired depth. This will greatly help the design survey field.

RESULTS AND DISCUSSION

This study measured the target at a depth of 2 cm with Dipole-dipole and Wenner configurations. Target block sizes are 20x5, 40x5, and 5x20. The 5x20 block is 5 cm in width and 20 cm in height. The 20x5 is 20 cm in width and 5 cm in height. Meanwhile, the 40x5 block is 40 cm in width and 5 cm in height.

Matching the curve

Good results were obtained from measurements of resistivity and chargeability on physical modeling created. The first reference to the theoretical shape of the curve is symmetrical. The symmetry measurement results were seen in all n. The results of all the curves on the target are coherent. The maximum amplitude of the curve lies at the midpoint, i.e., the top of the target. Between theoretical and measurement results show good agreement for all levels of iron-ore. Figure 2 is the theoretical and measuring curves at a 5x20 block target, 20% iron-ore content with Wenner configuration. A good correlation is shown by the results of measurement and theory. All the measurement curves show a positive correlation to iron- ore content in the target both for Dipole-dipole and Wenner configuration. It is found that the greater of iron-ore content of the measured block target, the greater the average amplitude of the chargeability measurement result.

The measurement of the resistivity parameter in the block target also shows a good result (Figure 2b). All the curves are coherent and symmetrical at zero point. The high response is observed in zero point at all n with amplitude fluctuation in the range of 30-50 Ohm-m. There is no significant amplitude variation of resistivity response to the changing of iron-ore content. At all iron-ore contents, the resistivity response shows a relatively constant value. The fluctuating amplitudes appear at a value of 37 Ohm-m on the left-right side consistently in all iron-ore contents which show resistivity value as host medium resistivity.

The amplitude of the theoretical resistivity curve decreases due to the value of target resistivity which is smaller than host medium resistivity. The theoretical results show the amplitude drops due to the value of host medium resistivity. The measurement resistivity curves show increases in amplitude. It is caused by the polarization phenomenon on the block target surface. The polarization effect on the highly conductive target which is sunk in the water

as a conductive host medium causes the resistivity value of the target to increase [25,26]. It commonly happens in physical modeling using host fluid or very conductive medium [14,15,17,27,28].
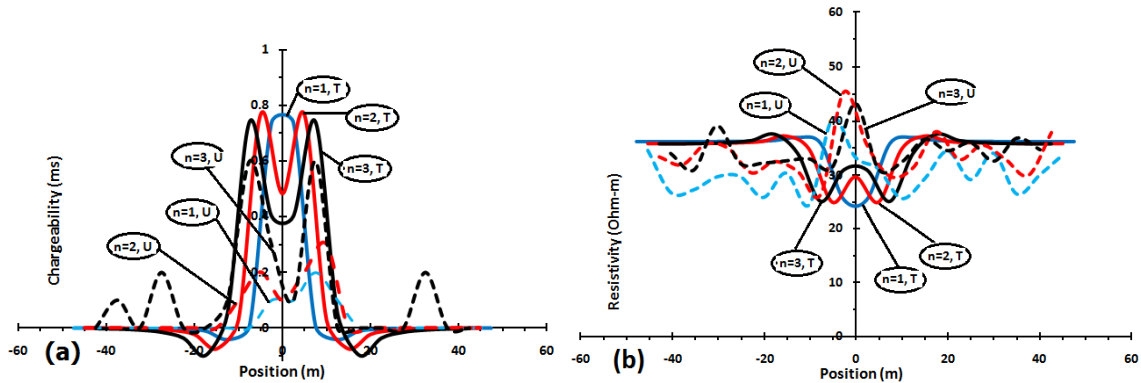

Figure 2. (a) The chargeability and (b)resistivity measurement curve and theoretical curve of the block target (5x20) with 20% iron-ore content, Wenner configuration, for n=1 to 3. n=1, T: theoretical curve for n=1 and n=1, U: measurement for n=1.

The curve matching with the measurement result in this research is done to assess the accuracy of physical modeling in describing the subsurface condition. The suitability of theoretical response and measurement is shown by the difference between both. The average difference of block target is 15.3% and 19.7% for Dipole-dipole configuration and 14.7% and 19.3% for Wenner configuration. The average difference between theoretical and measurement values in laboratory physical modeling in this research is less than 20%. It shows that the physical modeling which has been made in this research is quietly good. The difference in resistivity value is less than the chargeability value. In general, incompatibility on chargeability value is bigger than in resistivity value both on Dipole-dipole and Wenner configurations. It is caused by the accuracy of Syscal as a measurement tool used [22,29].

Inversion Modeling

One of the processing steps on IP measurement data is inversion to obtain true resistivity and chargeability value. The inversion of TDIP measured data in physical modeling is done by Res2DInv software [22,23]. The use of Res2DInv for inversion in this research is based on some considerations. First, the software resolution on block model distribution is used to generate the inversion initial model which affects the geometry interpretation [22]. In addition, the Res2DInv software is able to make the smallest block model as rectangular model with ¼ of side length from the smallest electrode space. The rules applied in laboratory physical modeling is 5 cm of space, thus, the smallest block model which can be generated by the software is a rectangular with size of 1,25 x 1,25 cm². The width of block model is 5 cm. Because of the block target size is bigger than 1.25 cm, the target dimension will be well detected. However, the software has some weaknesses, that is if the input data has large range, the inversion will be unstable, thus the damping factor should be upgraded. Also, it can cause quietly big RMS error [21,22].
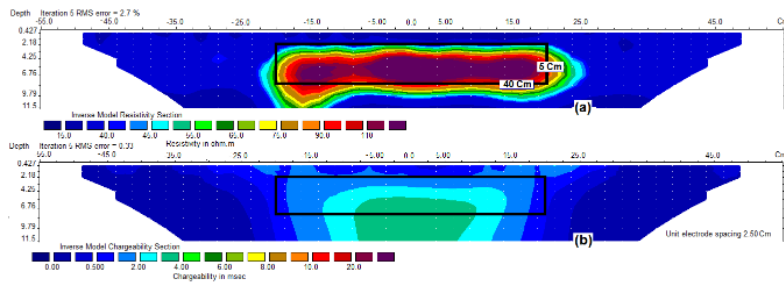
Figure 3. The example of inversion modeling (a) resistivity and (b) chargeability, block target (40x5), iron-ore content 40%, Dipole-dipole configuration, n=1-8. The rectangular line is the block target position

The resistivity value of the block is 16 Ohm-m and water is 36,63 Ohm-m. The inversion result for the 40x5 block model is shown in Figure 3. The result at block targets of 5x20 and 20x5 is almost the same. High anomalies appear precisely in the block position. The geometry boundaries are suitable for anomaly boundaries. The host medium around it has a value of 30-35 Ohm-m, making it suitable with the true resistivity value of water. The position and geometry of the target block can be obtained from the resistivity inversion. From these results, it can be stated that the physical modeling which has been made is quietly good because it can bring out subsurface parameters very well. Although the resistivity contrast of the block target and host medium is not too big, the position and geometry are described very well in the resistivity inversion modeling. The block target boundaries to the host medium are described as suitable with the anomaly boundaries. The chargeability inversion modeling shows a similar result. A high chargeability value indicates a high content of iron-ore. The high chargeability value is concentrated in the center part of the target. Resistivity inversion modeling is sensitive in describing geometry, while chargeability is more sensitive in describing distribution. The result of inversion modeling from the measured TDIP data also can be used to assess the effectiveness of laboratory physical modeling in describing the TDIP response behavior.
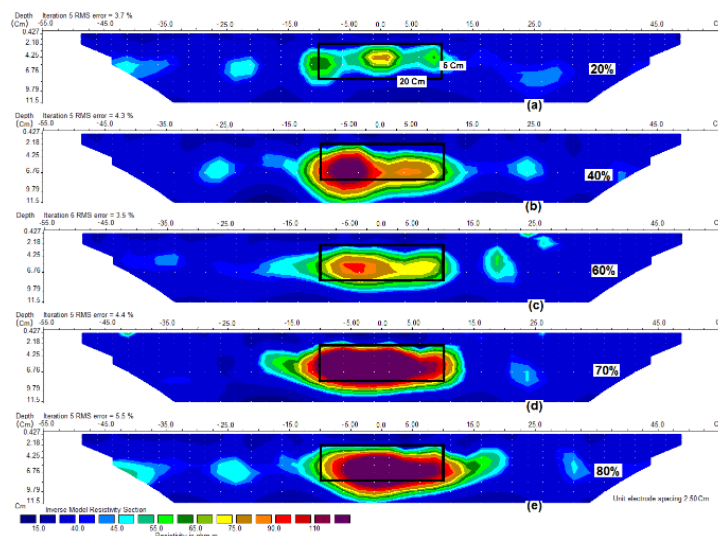

Figure 4. The result of inversion modeling with block target (20x5) for iron-ore content (a) 20%, (b) 40%, (c) 60%, (d) 70%, and (e) 80%, Dipole-dipole configuration; n=1-8. Rectangular line is the block target position in subsurface.

The measurement of TDIP response is carried out on block target with various content. The inversion modeling result of Dipole-dipole configuration with a 20x5 block target using iron-ore content of 20%, 40%, 60%, 70%, and 80% are shown in Figures 4 and 5 respectively.
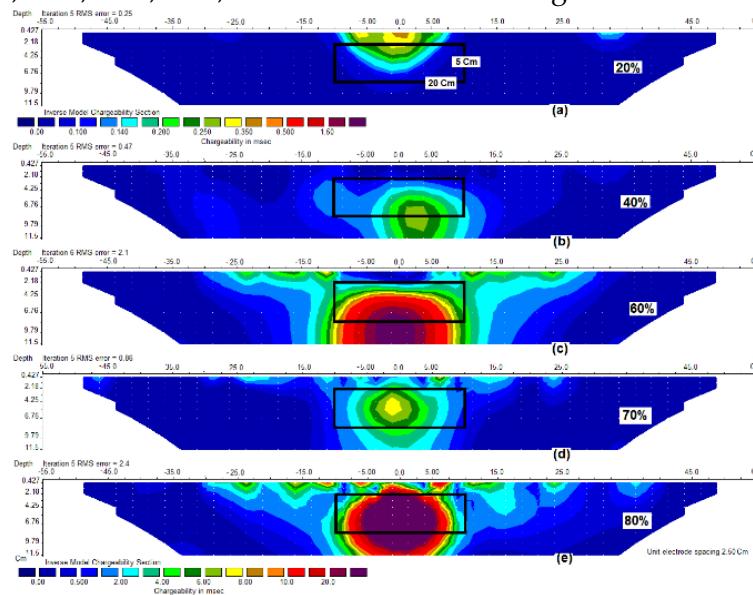

Figure 5. The chargeability inversion result with Dipole-dipole configuration, block target (20x5) for iron-ore content (a) 20%, (b) 40%, (c) 60%, (d) 70%, (e) 80%. The rectangular line is the block target position in the subsurface.

At all iron-ore contents, the resistivity anomalies appear very clear and consistent. The boundaries of resistivity anomaly precisely show the depth and block target geometry (Figure 4). In the inversion modeling of resistivity, block target resistivity and position are described very well. Resistivity changes due to the changing of iron-ore content at the block target. Its value ranges from 60 to 120 Ohm-m, meanwhile surrounding it is the host medium with various resistivity values from 15 – 40 Ohm-m. The result of resistivity inversion modeling for the 40x5 block target almost shows the same result.

Figure 5 is the result of chargeability inversion on the 20x5 target block with iron-ore content from 20% to 80% using the Dipole-dipole configuration. Chargeability anomaly is seen exactly in the block target position for all iron-ore content consistently. The width of the target is seen at all content and shown at values boundary of 2-6 ms. The high chargeability is located at the center of the target body for all iron-ore content. At Wenner configuration, the position and width of the block target appear in inversion modeling results. The chargeability parameter really shows the increased value due to the increase of mineral content in the target. The strongest chargeability anomaly is 80% of iron-ore content. The same result is found in the block target of 5x20 and 40x5. The result of resistivity inversion modeling always describes the target geometry and position. Chargeability inversion modeling, thus, can show the width and depth of the target, but it is not sensitive to geometry. The presence of consistency of chargeability anomaly changes due to the changes of iron-ore, showing that both are connected directly.

The Slicing of Inversion Modeling

The slicing at various depths from inversion modeling of measurement data is done to obtain a quantitative correlation of TDIP response to iron-ore content. The depth slicing is made by inversion modeling result as shown at Table 2. The slicing names for inversion modeling results are *d1-d8* for Dipole-dipole configuration and *w1-w8* for Wenner configuration.

This step is applied to all inversion results by using measurement data. The result of

inversion modeling is a block target with Dipole-dipole configuration and Wenner configuration for all iron-ore contents. The TDIP response curves to iron-ore content are obtained from all slices. For example, a slice of *d8* is chosen for the Dipole-dipole configuration because the slice is crossing through the center of the block (Figure 6).

Table 2. Depth incision inversion results

Dipole-dipole configuration		Wenner configuration	
Incision	Depth (cm)	Incision	Depth (cm)
d1	-0.214	w1	-0.313
d2	-0.427	w2	-0.625
d3	-1.282	w3	-1.875
d4	-2.179	w4	-3.188
d5	-3.166	w5	-4.631
d6	-4.252	w6	-6.219
d7	-5.446	w7	-7.966
d8	-6.759	w8	-9.888

From the curves in Figure 6a, it can be seen that the greater the iron-ore content in the block target, the greater the value of the TDIP response is, as shown by its amplitude. It occurs both on the Dipole-dipole configuration and Wenner configuration. The width of the curve indicates the width of the block target for the Dipole-dipole configuration. The curve at iron-ore content ranges from 20% to 80% are coherent with each other with maximum value at zero point. It shows that the strongest value of TDIP response is at the middle peak of the target and it is smaller on the side of the target with all iron-ore content. The results are suitable with the hypothesis that the greater the metallic mineral content, the greater the TDIP response is.
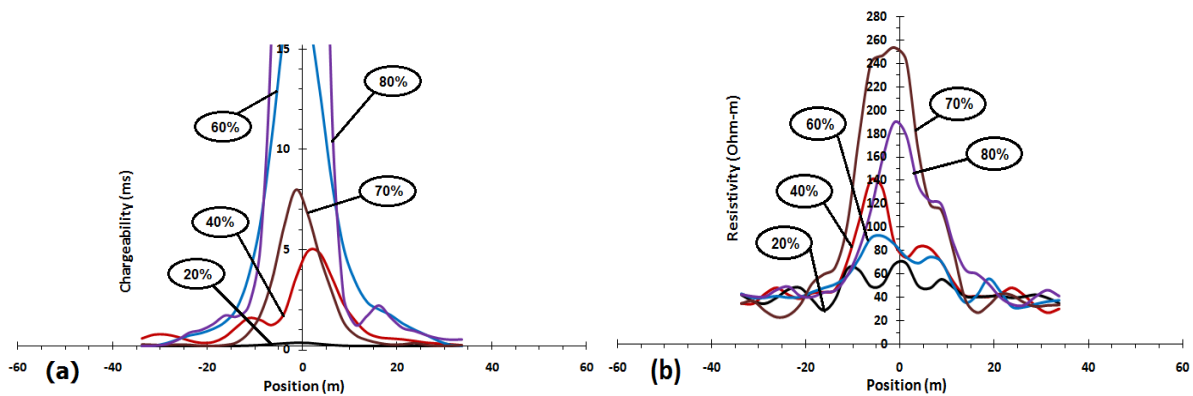

Figure 6. The curves of (a) chargeability and (b) resistivity of depth slicing *d8* for Dipole-dipole configuration. Laboratory physical modeling for block target (20x5) with iron-ore content 20%, 40%, 60%, 70%, and 80%.

The slice of the inversion resistivity curve in Figure 6b shows no specific pattern of the amplitude to iron-ore content. At ore contents of 20% and 40%, the amplitude increases. However, at the content of 60%, it decreases but it increases again at the iron-ore content of 70%. After that, it decreases again in the iron-ore content of 80%. The width of the curve shows the width of the target for the Dipole-dipole configuration. The slicing of chargeability and resistivity curves of the 5x20 and 40x5 block targets have also been generated as shown in Figure 6.
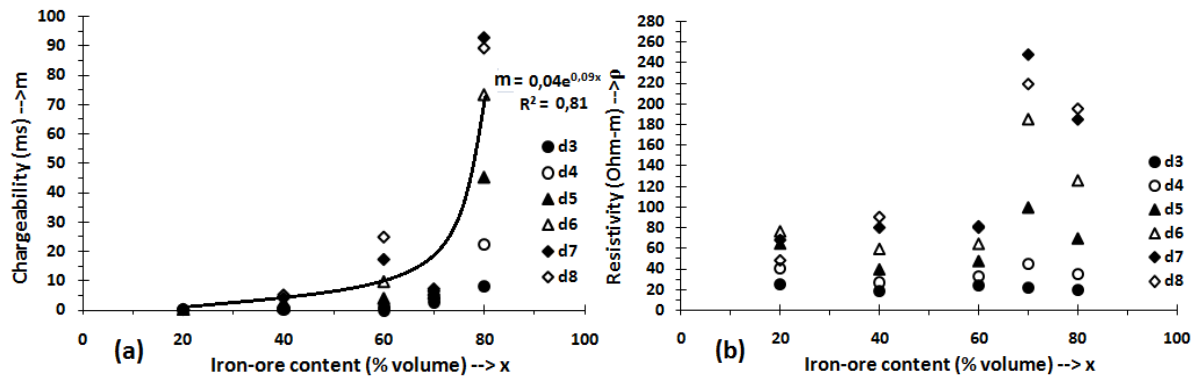
Figure 7. The graph correlates (a) chargeability and (b) resistivity to iron-ore content in 20x5 block target of Dipole-dipole configuration, at slicing *d8, d3* until *d8* of depth slicing.

The quantitative correlation between TDIP responses to the iron-ore content is obtained from the slicing of inversion results, shown in Figures 7a and 7b, as the result of chargeability and resistivity parameters. The curve in Figure 7a shows a coherent and congruent curve for all depths which are obtained from the Dipole-dipole configuration and Wenner configuration. The same values are shown on 20% of iron-ore content. It shows that the smaller of iron-ore content, the smaller the chargeability value will be and evenly spread in parts of target.

The graph of chargeability increases gradually from small iron-ore contents, starting from 70% and rapidly increases with slope more than 80%. The characteristics of that curve by Apparao and Sarma are expressed as the boundary of disseminated and massive minerals. The boundaries are obtained in this research is 70% of iron-ore content. If the iron-ore content in the target is less than 70%, that target is disseminated minerals. But if the target is greater than 70%, the target is massive minerals. If it is expressed in Fe-total, the boundary between disseminated and massive minerals in 25% of iron-ore contents will be obtained.

The similar curve as in Figure 7 is obtained for 5x20 and 40x5 block targets. However, the chargeability correlates exponentially to the of iron-ore contents (Table 3). All the curves are identical and show exponential correlation with different exponential index. From all the curves, the boundaries between massive and disseminated minerals showed 70% of iron-ore and 25% of Fe-total. The result of resistivity parameter is different as shown in Figure 7b, in which the resistivity value in all contents show almost the same values. It shows that the variable that affecting resistivity is not only dominated by metallic mineral contents. Porosity, clay content, temperature, and some factors do influence the resistivity value.

This research used resistivity value for target and host medium as shown in Table 1. The resistivity contrast ranges from 2.2 to 4.2 Ohm-m. The ideal resistivity contrast in the physical modeling is 100 [25]. Although the resistivity contrast is small, the results of inversion modeling for block target is quietly good. The linkage between resistivity and iron-ore content in the target cannot be obtained from laboratory physical modeling. The resistivity method is sensitive to determine the geometry, while the IP method is more sensitive to know the metallic mineral content in the subsurface. Because of that, in IP survey with metallic mineral target is difficult to be interpreted based on resistivity value only. To know the presence of metallic minerals in the survey area, it should be observed from the value and distribution of chargeability.

Table 3. The quantitative relationship chargeability to iron-ore and Fe-total content at block targets

Targets	Dipole-dipole Configuration		Wenner Configuration	
	Iron-ore (x)	Fe-total (x′)	Iron-ore (x)	Fe-total (x′)
Block (5x20)	m=0.11 exp (0.034)x	m=0.11 exp (0.097)x′	m=0.09 exp (0.02)x	m=0.09 exp (0.058)x′
Block (20x5)	m=0.04 exp (0.09)x	m=0.04 exp (0.26)x′	m=0.21 exp (0.055)x	m=0.21 exp (0.16)x′
Block (40x5)	m=0.92 exp (0.032)x	m=0.92 exp (0.09)x′	-	-

m: chargeability (ms), x and x′: iron-ore and Fe-total content (% volume)

CONCLUSION

The theoretical curves which have been derived from the mathematical formulation of the subsurface model are suitable to be used as examiners for the success of laboratory physical modeling. The test result shows that the laboratory physical modeling which has been made is quietly good. The result of inversion modeling on the block model also shows a similar result. Because of that, the physical modeling which has been made is effective to understand the behavior of TDIP response. The subsurface parameter includes position and geometry which can be identified by the result of inversion modeling from laboratory physical modeling data. The resistivity inversion modeling is more sensitive to identifying the geometry and position of the target, while the chargeability inversion is more sensitive to identify the distribution of metallic minerals in the target. From the result of laboratory physical modeling, the boundary of disseminated and massive minerals can be obtained with an amount of 70% in iron-ore. This research obtains a quantitative correlation between chargeability and iron-ore content in several targets with Dipole-dipole and Wenner configurations. Both are connected exponentially with a different exponential index for a different target. Meanwhile, the correlation between resistivity and metallic mineral content in the target has not been obtained quantitatively from physical modeling. The handling procedure of physical modeling has been resulted for the time domain IP method and to determine the correlation between TDIP responses to the iron-ore content. This procedure is expected to become standard procedure for handling the physical modeling of the IP method in the time domain.

AUTHOR CONTRIBUTIONS

Yatini: Conceptualization, Methodology, and Validation; Djoko Santoso: Methodology, Formal Analysis; Budi Sulistijo: Resources, and Writing - Original Draft; and Agus Laesanpura: Data Curation, Project Administration, and Writing - Original Draft.

DECLARATION OF COMPETING INTEREST

The authors declare that they have no known competing financial interests or personal relationships that could have appeared to influence the work reported in this paper.

REFERENCES

[1] Evrard M, Dumont G, Hermans T, Chouteau M, Francis O, Pirard E, and Nguyen F. Geophysical Investigation of the Pb–Zn Deposit of Lontzen–Poppelsberg, Belgium. *Minerals*. 2018; **8**(6): 233. DOI: https://doi.org/10.3390/min8060233.

[2] Dusabemariya C, Qian W, Bagaragaza W, Faruwa A, and Ali M. Some experiences of resistivity and induced polarization methods on the exploration of sulfide: A review. *Journal of Geoscience and Environment Protection*. 2020; **8**(11): 68-92. DOI: https://doi.org/10.4236/gep.2020.811004.

[3] Taha A, Ismail A, Massoud U, Mesbah H, and Komarov V. Induced Polarization Measurements for Gold Exploration at the Eastern Desert of Egypt. *Bulletin of Earth Sciences of Thailand*. 2021; **2**(1): 20–30. Available from: https://ph01.tci-thaijo.org/index.php/bestjournal/article/view/246464.

[4] Mau D, Revil A, and Hinton J. Induced polarization response of porous media with metallic particles—Part 4: Detection of metallic and nonmetallic targets in time-domain-induced polarization tomography. *Geophysics*. 2016; **81**(4): D359–D375. DOI: https://doi.org/10.1190/geo2015-0480.1.

[5] Yatini Y, Santoso D, Laesanpura A, and Sulistijo B. Physical Modeling on Time Domain Induced Polarization (TDIP) Response of Metal Mineral Content. *Indonesian Journal of Applied Physics*. 2018; **8**(2): 57–66. DOI: https://doi.org/10.13057/ijap.v8i1.20648

[6] Dakir I, Benamara A, Aassoumi H, Ouallali A, and Bahammou YA. Application of induced polarization and resistivity to the determination of the location of metalliferous veins in the Taroucht and Tabesbaste areas (Eastern Anti-Atlas, Morocco). *International Journal of Geophysics*. 2019; **2019**: 5849019. DOI: https://doi.org/10.1155/2019/5849019.

[7] Gurin G, Titov K, Ilyin Y, and Tarasov A. Induced polarization of disseminated electronically conductive minerals: a semi-empirical model. *Geophysical Journal Internasional*. 2015; **200**(3): 1555–1565. DOI: https://doi.org/10.1093/gji/ggu490.

[8] Essa KS and Munschy M. Mineral Exploration from the Point of View of Geophysicists. In *Minerals*. London: IntechOpen; 2019. DOI: https://doi.org/10.5772/intechopen.84830.

[9] Araffa SA, Mansour SA, Santos FM, and Helaly A. Geophysical exploration for gold and associated minerals, case study: Wadi El Beida area, South Eastern Desert, Egypt. *Journal of Geophysics and Engineering*. 2009; **6**(4): 345–356. DOI: https://doi.org/10.1088/1742-2132/6/4/002.

[10] Alfouzan FA, Alotaibi AM, Cox LH, and Zhdanov MS. Spectral induced polarization survey with distributed array system for mineral exploration: Case study in Saudi Arabia. *Minerals*. 2020; **10**(9): 769. DOI: https://doi.org/10.3390/min10090769.

[11] Maurya PK, Balbarini N, Moller I, Ronde V, Christiansen AV, Bjerg PL, Auken E, and Fiandaca G. Subsurface imaging of water electrical conductivity, hydraulic permeability and lithology at contaminated sites by induced polarization. *Geophysics Journal Internasional*. 2018; **213**(2): 770–785. DOI: https://doi.org/10.1093/gji/ggy018.

[12] Revil A, Ahmed AS, Coperey A, Ravanel L, Sharma R, and Panwar N. Induced polarization as a tool to characterize shallow landslides. *Journal of Hydrology.* 2020; **589**: 125369. DOI: https://doi.org/10.1016/j.jhydrol.2020.125369.

[13] Olsson PI, Fiandaca G, Maurya PK, Dahlin T, and Auken E. Effect of current pulse duration in recovering quantitative induced polarization models from time-domain full-response and integral chargeability data. *Geophysical Journal Internasional*. 2019; **218**(3): 1739–1747. DOI: https://doi.org/10.1093/gji/ggz236.

[14] Li J, Liu JX, Tong XZ and Guo ZW. The Physical Modeling Experiments Analysis of the

Exploration Depth of Conventional Electric Survei. *PIERS Proceedings. Xi'an. China*, 2010. DOI: https://doi.org/10.13057/ijap.v8i1.20648

[15] Devi PP, Prasad PR, Rajesh R, Padalu G and Sarma VS. Efficacy of electrode arrays in resistivity prospecting using physical modelling. *The Journal of Indian Geophysical Union.* 2014; **18**(1): 85–97.

[16] Yatini Y, Santoso D, Laesanpura A, and Sulistijo B. Studi Pemodelan Respon Polarisasi Terinduksi dalam Kawasan Waktu (TDIP) terhadap Kandungan Mineral Logam, Sebuah Hasil Awal. *Indonesian Journal of Applied Physics.* 2017; **4**(2): 162–170. DOI: https://doi.org/10.13057/ijap.v4i02.4984

[17] Yatini Y, Santoso D, and Laesanpura A. Physical Modeling Studies of the Time Domain Induced Polarization (TDIP) Response, Case: Homogeneous Isotropic Medium. *Proceedings 3rd Annual Basic Science International Conference (BaSIC).* Malang: Universitas Brawijaya Malang; 2013. Available from: http://eprints.upnyk.ac.id/18691/1/2013-Basic.pdf

[18] Kingman JEE, Ritchie TJ, and Rowston P. Induced polarization chargeability calibration standards. *ASEG Extended Abstracts*. 2019; **2019(**1): 1–5. DOI: https://doi.org/10.1080/22020586.2019.12073143.

[19] Turai E, Turtogtokh B, Dobróka M, and Baracza MK. Newer results of Monte Carlo inversion of IP data in water base protection and ore exploration. *Acta Geodaetica et Geophysica*. 2021; **56**(4): 667–679. DOI: https://doi.org/10.1007/s40328-021-00352-6.

[20] Mary B, Saracco G, Peyras L, Vennetier M, Meriaux P, and Camerlynck C. Mapping tree root system in dikes using induced polarization: Focus on the influence of soil water content. *Journal of Applied Geophysics*. 2016; **135**: 387–396. DOI: https://doi.org/10.1016/j.jappgeo.2016.05.005.

[21] Loke MH, Chambers JE, and Ogilvy RD. Inversion of 2D spectral induced polarization imaging data. *Geophysical Prospecting*. 2006; **54**(3): 287–301. DOI: https://doi.org/10.1111/j.1365-2478.2006.00537.x.

[22] Loke MH, Chambers JE, Rucker DF, Kuras O, and Wilkinson PB. Recent developments in the direct-current geoelectrical imaging method. *Journal of Applied Geophysics.* 2013; **95**: 135–156. DOI: https://doi.org/10.1016/j.jappgeo.2013.02.017.

[23] Loke MH. *Tutorial: 2-D and 3-D electrical imaging surveys*; 2004. Available from: https://sites.ualberta.ca/~unsworth/UA-classes/223/loke_course_notes.pdf.

[24] Yatini Y and Laesanpura A. Influence of potential's electrode selection on physical modeling of time domain induced polarization (TDIP), case studies of homogeneous isotropic medium. *AIP Conference Proceedings*. 2013; **1554**(1): 245–248. DOI: https://doi.org/10.1063/1.4820331.

[25] Apparao A, Srinivas GS, Sarma VS, Thomas PJ, Joshi MS, and Prasad PR. Depth of detection of highly conducting and volume polarizable targets using induced polarization. *Geophysical Prospecting*. 2001; **48**(5): 797–813. DOI: https://doi.org/10.1046/j.1365-2478.2000.00212.x.

[26] Ward SH. *The resistivity and induced polarization methods*. In *Geotechnical and Environmental Geophysics.* Tulsa: Society of Exploration Geophysicists. 1990; 147-190. DOI: https://doi.org/10.1190/1.9781560802785.ch6.

[27] Jougnot D, Ghorbani A, Revil A, Leroy P, and Cosenza P. Spectral induced polarization of partially saturated clay-rocks: A mechanistic approach. *Geophysical Journal Internasional*. 2010; **180**(1): 210–224. DOI: https://doi.org/10.1111/j.1365-246X.2009.04426.x.

[28] Gainullin IK. Theoretical investigation of the ion-induced polarization-charge influence on resonant charge transfer. *Physical Review A*. 2019; **100**(3): 032712. DOI:

https://doi.org/10.1103/PhysRevA.100.032712.

[29] Dahlin T and Loke M H. Negative apparent chargeability in time-domain induced polarisation data. *Journal of Applied Geophysics*. 2015; **123**: 322–332. DOI: https://doi.org/10.1016/j.jappgeo.2015.08.012.